Article
Vol. 22, No. 6, p. 1069–1080, December 2018
https://doi.org/10.1007/s12303-018-0050-z
pISSN 1226-4806 eISSN 1598-7477
Geosciences Journal GJ

Analysis of the relationship between volcanic eruption and surface deformation in volcanoes of the Alaskan Aleutian Islands using SAR interferometry

Seulki Lee and Chang-Wook Lee*

Division of Science Education, Kangwon National University, Chuncheon, Gangwon-do, 24341, Republic of Korea

ABSTRACT: The Alaskan Aleutian Islands form one of the world's largest volcanic island chains. The islands are exposed to both direct and indirect damage from continuous volcanic eruptions. Surface deformation is mostly observed before volcanic eruption, but with some volcanoes, such as Ontake Volcano, deformations cannot be detected. In this study, we analyzed volcanic eruptions in the Alaskan Aleutian Islands, which is a region of frequent volcanic eruptions. Based on our results, we predicted the type of eruption that would occur on Baekdusan Volcano according to the presence or absence of surface deformation. For this purpose, 10 sites were selected from areas where recent volcanic activity had occurred in the Aleutian Islands. Additionally, Advanced Land Observing Satellite Phased Array-type L-band Synthetic Aperture Radar (ALOS-PALSAR) and European Remote Sensing (ERS)-1/2 satellite data were obtained from 10 experimental sites. Based on the radar satellite data, the volcanic surface deformations were identified, and the characteristics of the volcanic eruption were quantitatively calculated by determining the presence of surface deformation. The results of this study should facilitate the process of correlation between volcanic eruption and surface deformation.

Key words: surface deformation, volcanic eruption, SAR interferometry

Manuscript received May 17, 2018; Manuscript accepted September 17, 2018

1. INTRODUCTION

Natural disasters, such as earthquakes and volcanic eruptions, occur suddenly. These disasters cause severe damage and are very difficult to predict in advance. In particular, lava flows and volcano clusters that appear during a volcanic eruption cause secondary problems such as landslides and tsunamis, as well as the destruction of cities, farmland, and vegetation, resulting in considerable loss of life and economic damage. In addition to inducing respiratory illness among local residents, volcanic eruptions cause other problems such as disrupting air traffic. The Aleutian region is one of the largest volcanic island chains in the world, and experiences direct and indirect damage due to constant volcanic eruptions (Fig. 1).

The active volcanoes in the Aleutian region have different forms and are irregularly dispersed, which makes it difficult to predict the timing of eruptions. Data for accurately predicting these eruptions would provide important information for analyzing volcanoes around the world. Numerous studies have been conducted on the Alaskan Aleutian volcanoes (Waythomas and Waitt, 1998; Miller et al., 1998; Lu et al., 2005a; Begét and Kowalik, 2006; Waitt and Begét, 2009); However, few studies have examined volcanic activity across the entire Aleutian Islands chain. Remote sensing is an important tool in volcano monitoring due to the large spatial extent of potential eruption pre-cursor signals. Interferometric synthetic aperture radar (InSAR) is a remote sensing technique for measuring ground surface deformation with sub-centimeter precision at a spatial resolution of tens of meters over a large area. InSAR technology has been used to rapidly measure and monitor the surface deformation status of disturbance episodes on all the Aleutian volcanoes over a wide area to predict volcanic activity, which can be used in probabilistic analysis of changes in the magmatic plumbing system to provide information and warnings on potentially dangerous situations (Biggs et al., 2014). Therefore, we applied the InSAR technique to the Aleutian Islands to observe the presence or absence of

*Corresponding author:
Chang-Wook Lee
Division of Science Education, Kangwon National University, 1 Kangwondaehak-gil, Chuncheon, Gangwon-do, 24341, Republic of Korea
Tel.:+82-33-250-6731, E-mail: cwlee@kangwon.ac.kr

surface deformation due to volcanic activity in a region that has experienced the most active eruption history in the world. Subsequently, we calculated the probability of eruption based on the surface deformation observed in this study at Baekdusan Volcano.

Surface displacement, a phenomenon associated with volcanic eruptions, is generally observed before an eruption, but may not occur depending on the characteristics of the volcanic rock (e.g., Mount Ontake). In this study, we investigate volcanic eruptions in the Aleutian archipelago, which occur frequently, and make predictions regarding the types of eruption that will occur at the Baekdusan Volcano according to the presence or absence of surface displacement. For this purpose, 10 sites of volcanic activity were identified, for which Advanced Land Observation System (ALOS) phased-array synthetic aperture radar (PALSAR) satellite data were obtained.

2. STUDY AREA AND GEOLOGICAL SETTING

Alaska is one of the world's most active volcanic regions, containing 268 volcanoes. There are differentiation records for 158 of these volcanoes, of which 69 are classified as active (Lu et al., 2005a). The differentiation records and characteristics of the 10 study areas in the Aleutian Islands were analyzed, as shown in Table 1; differentiation had occurred in all these areas since 2005. Figure 1 shows the locations of the volcanoes.

Redoubt Volcano is a 3,108-m stratovolcano-type volcano located at 60°29′07″N, 152°44′35″W, approximately 170 km southwest of Anchorage in Clark National Park. Redoubt began showing signs of activity in September 2008, which increased steadily until 2009; heat was detected near the crater. The 2009 eruption began with a minor ash-and-steam explosion. The emissions originated from a new vent, located just south of the 1990 lava dome and west of the prominent ice collapse feature near the north edge of the summit crater. The eruption lasted for 17 minutes and featured lahar flow, with volcanic material deposited on March 23. Alaska Airlines canceled 19 flights due to this eruption. Shishaldin is located at 54°45′21″N, 163°58′03″W; it is the most symmetrical volcano in this study and has a height of 2,857 m. Shishaldin comprises three large stratovolcanoes. The most-recent eruption of Shishaldin began in January 2014 and continued until March 2015. Volcanic activity increased on January 28, 2014, and the eruption of lava in normal craters was reduced by mid-March (Alaska Volcano Observatory; AVO). Volcanic activity has not been observed since January 13, but a slightly elevated surface temperature was detected. Shishaldin showed a steady decrease in thermal activity in the months prior to an AVO report on March 10, 2016, at which time volcanic eruptions were no longer occurring, and the warning level was thus lowered to normal. Continuous observation of Shishaldin is necessary as it is a frequently erupting volcano, although it has not yet caused loss of life or property. Augustine Island is a stratovolcanic island with an elevation of 1,260 m and an area of 90 km^2, located approximately 290 km southwest of Anchorage, Alaska, USA (Kienle and Shaw, 1979; Waythomas and Waitt, 1998). The Aleutian archipelago, wherein Augustine is located, contains about 57 volcanoes where the Pacific and North American plates meet. Augustine is among the most active of these volcanoes (Miller et al., 1998; Begét and Kowalik, 2006; Waitt and Begét, 2009). Okmok is a 1,073-m volcano at 53°28′05″N, 168°10′30″W, northeast of Umnak Island. It is a basalt volcanic complex occupying most of the northeastern part of the central

Table 1. Characteristics of the active volcanoes in this study

	Volcano	Latitude	Longitude	Height (m)	Last eruption	Rock type	VEI	Description
1	Redoubt	60.48	152.74	3,108	2009 03-15	An/BaAn/Ba/Pi-Ba	3	A.H. ~SE 15.2 km, Lahar ~35 km, Ashfall ~NE 545 km, Ash plume ~4.6 km
2	Veniaminof	56.19	159.39	2,507	2013 06-13	An/BaAn/Ba/Pi-Ba/Da	3	A.H. ~4.6 km, Drift ~NW
3	Shishaldin	54.75	163.97	2,857	2014 01-28	Ba/Pi-Ba/An/BaAn	1	S.P. ~300 m, Drift ~SE 16–25 km
4	Augustine	59.36	153.43	1,260	2005 12-01	An/BaAn/Da	3	A.H. ~9 km, Earthquake 20–35/d, Drift ~SE 80 km
5	Makushin	53.89	166.92	1,800	1995 01-30	An/BaAn/Ba/Pi-Ba/Tr/ BaTr/Da	1	A.H. ~2.4 km, Drift ~NE
6	Okmok	53.41	168.13	1,073	2008 07-12	Ba/Pi-Ba/An/BaAn	4	A.H. ~15.2 km, Drift ~NE 105 km, NE caldera floor
7	Cleveland	52.82	169.94	1,730	2014 06-05	An/BaAn/Da		A.H.~6 km, Drift ~SE 10 m/s
8	Seguam	52.31	172.51	1,054	1993 08-19	An/BaAn/Da/Ba/Pi-Ba	2	A.H. 0.9~1.2 km,
9	Korovin	52.37	174.15	1,533	2005 02-23	Ba/Pi-Ba/An/BaAn/Da	1	A.H. ~2.4 km, Drift ~E
10	Kanaga	51.92	177.16	1,307	2012 02-18	An/BaAn/Tr/BaTr/Da/ Ba/Pi-Ba	2	Earthquake, Drift ~NE 39 km

Rock type: An: andesite, Ba: basalt, BaAn: basaltic andesite, BaTr: basaltic trachyandesite, Da: dacite, Pi-Ba: picrobasalt, Rhy: rhyolite, Tr: trachyandesite.
Description: A.H.: ash height, S.P.: steam plume.

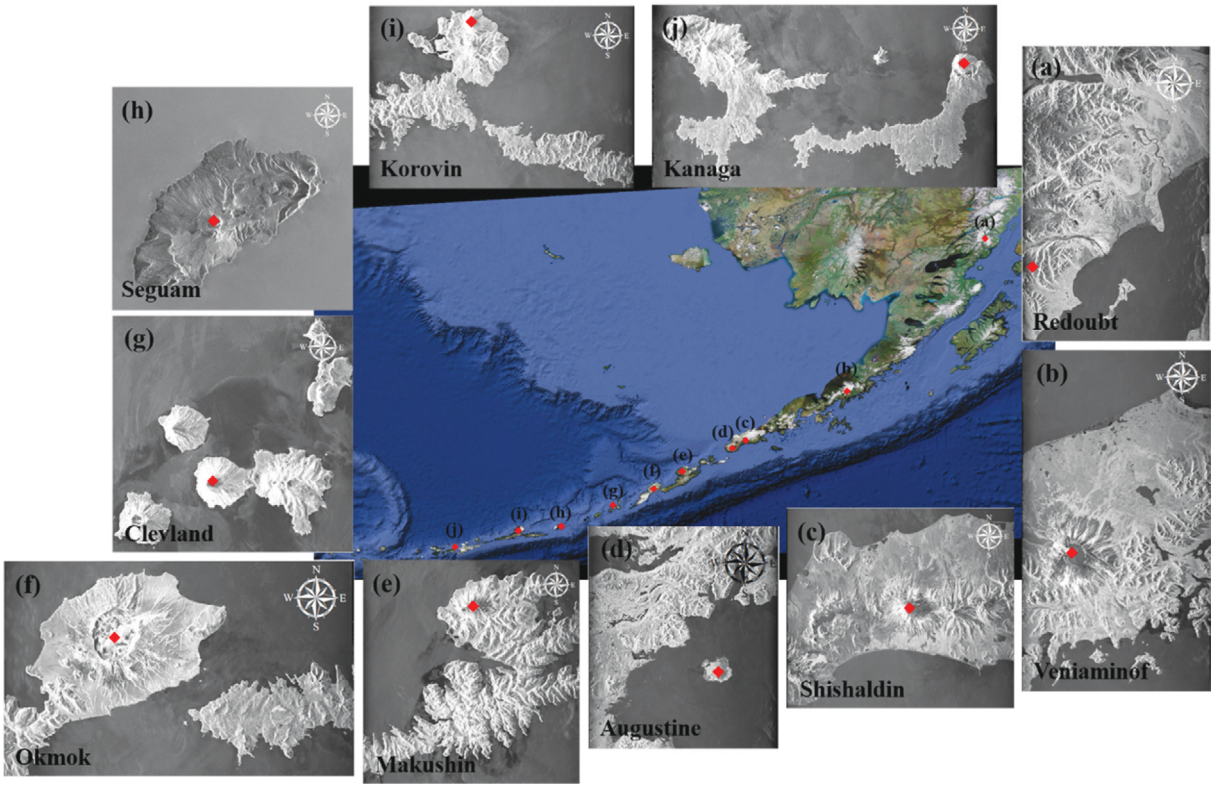

Fig. 1. Locations of the Alaskan volcanoes in this study: (a) Redoubt, (b) Veniaminof, (c) Shishaldin, (d) Augustine, (e) Makushin, (f) Okmok, (g) Cleveland, (h) Seguam, (i) Korovin, and (j) Kanaga.

Aleutian volcanic crater and has a 9.3-km caldera at its top. A volcanic earthquake of 2–3.6 M was observed in May 2001 but did not lead to an eruption. However, on July 12, 2008, an eruption began with a sudden volcanic earthquake. During the early part of the eruption, volcanic gas and ash were released in a cloud up to 15 km high, which then spread southward and eastward. The volcanic ash cloud was at a height of 7.6–9.1 km on July 19, and spread to the southeast over an area of about 20 km at an altitude of 3.7 km. On August 9–10, the volcanic ash was at a height of 4.6 km, rising to 6.1 km on August 11 and spreading southeast. Since then, the seismic and volcanic activities have gradually decreased (Lu et al., 2005). Cleveland is a stratovolcano-type volcano 1,730 m in height. It is located toward the western end of Chuginadak Island, which is one of four islands comprising the Aleutian archipelago; it is among the most active volcanoes in the archipelago. Many water systems on the steep side of Cleveland were generated by lava flows (Miller et al., 1998). Cleveland experienced frequent small-scale differentiations between 2005–2009 and 2011–2013 (McGimsey et al., 2007; Neal et al., 2011; De Angelis et al., 2012; Guffanti and Miller, 2013). Small-scale eruptions of Cleveland require observation and have continued to occur throughout 2015. Korovin Volcano is a 1,530-m high volcano located at 52°22′49″N, 174°10′06″W, and with a record of volcanic activity between 1998 and 2007. Beginning on June 30, 1998, eruption activity was observed for about 1 month and a cloud of ash rose up to 9.1 km. Volcanic activity was observed through July (McGimsey et al., 2003). Volcanic activity was also observed in July 2002, but caused no direct damage (McGimsey et al., 2007). Kanaga is a 1,307-m high volcano on Andreanof Island in the Aleutian Archipelago, with a volcanic fumarole located in its northeast portion and a small lake on the bottom of an older caldera in its southeast portion. A large-scale earthquake of 6.6 M was recorded in 2008 (Dixon and Stiher, 2009).

3. METHODOLOGY

3.1. Small Baseline Subset (SBAS) Processing

Advanced Land Observing Satellite Phased Array-type L-band Synthetic Aperture Radar (ALOS-PALSAR) satellite image data were collected in the study area. Differential interferometric SAR (DInSAR) images were generated based on ALOS-PALSAR images from 2006 to 2011 and the SBAS time-series algorithm was applied (Ferretti et al., 2000, 2001; Berardino et al., 2002; Kim et al., 2010; Lee et al., 2010, Kim and Cho, 2011).

DInSAR is a technique that is used to observe surface deformations in two dimensions over a wide area (several tens

https://doi.org/10.1007/s12303-018-0050-z

of square kilometers) offering a sensitivity of millimeters to centimeters. Initially, the DInSAR technique was limited to examining surface deformations caused by a one-time event from a pair of differential interferometric images. However, the use of just a single pair of interferograms to determine the presence or absence of surface deformation on the summits of volcanoes is unreliable because of atmospheric effects related to tropospheric delay. Moreover, it is difficult to quantitatively measure the deformation at the same point due to temporal and baseline decorrelation when analyzing differential interferometric images for different periods. Therefore, recent research trends have shifted to observe surface deformation over time using different SAR image data from regions around the world.

The SBAS algorithm can calculate surface deformation (Hong et al., 2010; Kim, 2012; Yang et al., 2014; Lee et al., 2017) from the SAR images using time-series analysis corresponding to values relative to a reference point (in this study, a pixel location was used to reference interferogram phase values) (Lee et al., 2012). In addition, each phase component is separated from the differential interference, including the error signal in the orbit used, and delays caused by atmospheric signals or noise. To apply the SBAS algorithm, an interferometric map is used with only minor decorrelation effects over short distances and time intervals. In this study, we applied an improved version of a previous SBAS algorithm (Jung et al., 2007, 2008).

In this study, the SBAS algorithm was used to observe the displacement over time using short images with a length of 100–150 m along the vertical baseline to eliminate the spatial decorrelation caused by the differential interferogram (Berardino et al., 2002). In this algorithm, a differential interferogram that is not connected in time due to the limitation of the vertical baseline occurs; a singular value decomposition (SVD) method was used to address this. Additionally, a residual differential interferogram was used to minimize the unwrapping error, and a low- and high-pass filter was applied spatially to compensate for the atmospheric effects of each differential interferogram. We used a complementary SBAS algorithm using finite difference approximation to remove the noise component of the surface deformation in the existing SBAS algorithm. Furthermore, we were able to measure the presence or absence of surface deformation using ERS-1/2 (1993–2001) and ALOSPALSAR (2007–2011) data with refined SBAS time-series results classified into cases of eruption corresponding to deformed and not-deformed by volcanic activity from the magma plumbing system.

3.2. Positive and Negative Predictive Values

Positive predictive values and negative predictive values (PPVs and NPVs, respectively) are statistics used primarily in the medical field in the context of diagnosing pathologies, and especially to detect early stage disease in patients with a relatively low probability of developing a particular condition, rather than in symptomatic individuals. The PPV and NPV denote diagnostic accuracy by predicting the occurrence probability of an event within a group unlikely to experience that event (Parikh et al., 2008; Biggs et al., 2014).

Table 2 shows the method for determining positive and negative predictive values. The sensitivity is the probability that surface deformation is detected when there is a volcanic eruption. Specificity is the probability that there is surface deformation in an area where there are no volcanic eruptions. The PPV is the probability that eruption actually occurs in a group of volcanoes predicted to show eruption. The NPV is the probability of there being no eruption in a group of volcanoes predicted to show no eruption. Volcanic eruptions and surface displacements in a volcanic area can be expressed in these terms using Equations (1)–(4).

$$\text{Sensitivity} = \frac{\text{Number of true positives}}{\text{Number of true positives} + \text{Number of false negatives}}, \quad (1)$$

$$\text{Specificity} = \frac{\text{Number of true negatives}}{\text{Number of false positives} + \text{Number of true negatives}}, \quad (2)$$

$$\text{PPV} = \frac{\text{Number of true positives}}{\text{Number of true positives} + \text{Number of false positives}}, \quad (3)$$

$$\text{NPV} = \frac{\text{Number of true negatives}}{\text{Number of false negatives} + \text{Number of true negatives}}. \quad (4)$$

Here, true positive represents detection of surface deformation with volcanic eruption; false negative represents no surface deformation with volcanic eruption; false positive is detection of surface deformation with no volcanic eruption; and true negative

Table 2. Method for determining positive and negative predictive values

	Eruption	No Eruption
Surface deformation	Presence of surface deformation with eruption (A) – (true-positive)	Presence of surface deformation with no eruption (B) – (false-positive)
No surface deformation	No change in surface deformation with eruption (C) – (false-negative)	No change in surface deformation with no eruption (D) – (true-negative)

is no surface deformation and no eruption.

4. RESULTS AND DISCUSION

In this study, surface deformation was observed on 10 volcanic islands, as shown in Table 3, by applying the SBAS algorithm described in Section 3.1. to predict the probability that surface displacement would be observed. Figures 2–7 show the results of time-series analyses performed using the SBAS algorithm for the 10 study volcanoes. In this study, we used ALOS-PALSAR and ERS-1/2 data (Table 4).

Therefore, we defined a reference point on stable area where we assumed to be absent surface deformation (relatively zero phase when compared to other points) occurred due to the volcanic activities with maintain high coherence. We used a map of average deformation per year to set the point where no deformation appeared as the reference point.

4.1. Redoubt Volcano

Figure 2a shows the location of Redoubt Volcano and Figure 2b is the time-series of surface displacement near the volcano. Time-series analysis around the volcano shows subsidence after July 2009, followed by an increase in surface level. Redoubt Volcano erupted in 2009, and then rose slowly after subsidence. Thus, Redoubt Volcano can be regarded as exhibiting surface displacement due to eruption.

4.2. Augustine Volcano

Figure 3a shows the location of Augustine Volcano, Figure 3b is the time-series of surface displacement based on various observation points, Figure 3c is the differential interferometric map, and Figure 3d is the time-series of deformation. Displacement appears to increase steadily in Augustine, but no volcanic activity

Table 3. Positive and negative predictive values for the volcanoes in this study

	Volcano	Eruption	Surface Deformation	Deformation 2007–2012	PPV/NPV[(a)]
1	Redoubt	Eruption (‘09)	Deformation	Yes (‘07–‘12)	T.P.
2	Veniaminof	Eruption (‘04–‘08)	Deformation	Yes (‘09–‘12)	T.P.
3	Shishaldin	Eruption (‘08)	Deformation	Yes (‘09–‘12)	T.P.
4	Augustine	No Eruption	Deformation	Yes (‘07–‘12)	F.P.
5	Makushin	No Eruption	Deformation	Yes (‘09–‘12)	F.P.
6	Okmok	Eruption (‘08)	Deformation	Yes (‘07–‘10)	T.P.
7	Cleveland	Eruption	Deformation	Yes (‘09–‘12)	T.P.
8	Seguam	No Eruption	Deformation	Yes (‘92–‘10)	F.P.
9	Korovin	Eruption (‘06)	Deformation	Yes (‘07–‘12)	T.P.
10	Kanaga	No Eruption	No Deformation	No	T.N.

[(a)] T.P.: true-positive; F.P.: false-positive; F.N.: false-negative; T.N.: true-negative.

Table 4. SAR interferograms used in this study

Satellite	Band	Path	SLC image	Interferogram
ALOS-PALSAR	L-band	263–293	255	361
ERS-1/2	C-band	201,473	60	76

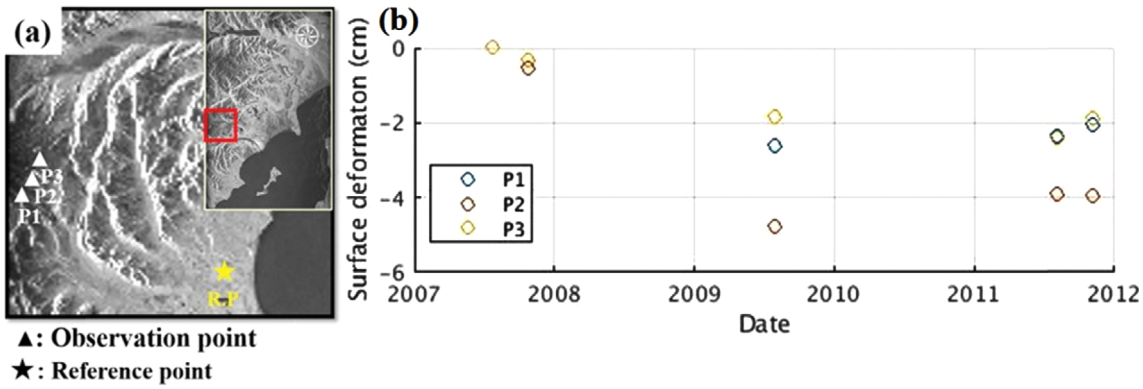

Fig. 2. Results for Redoubt Volcano; (a) location of Redoubt Volcano using SAR data, (b) surface deformation at the observation point.

https://doi.org/10.1007/s12303-018-0050-z

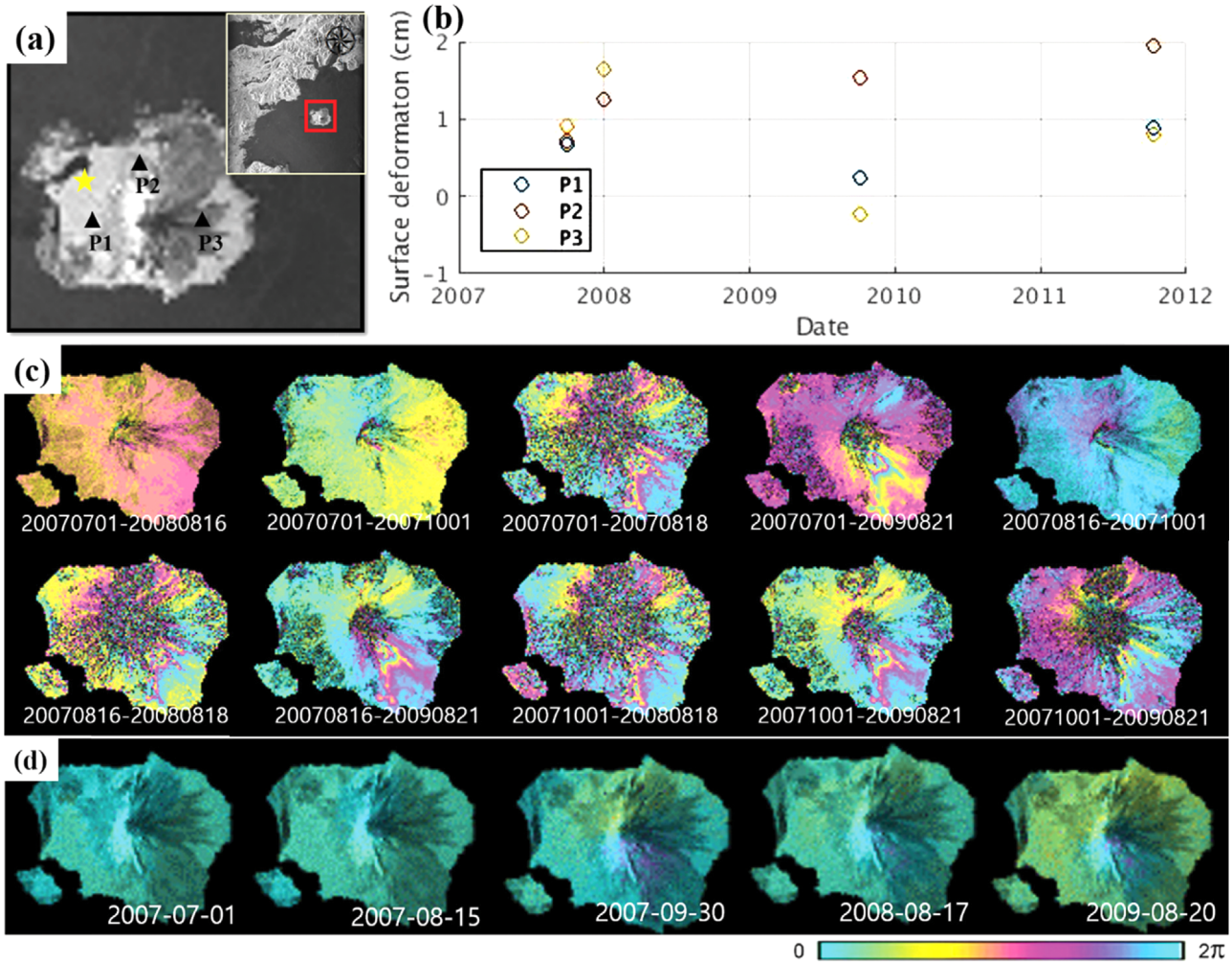

Fig. 3. Results for Augustine Volcano; (a) location of Augustine Volcano using SAR data, (b) surface deformation at the observation point, (c) differential interference map using ALOS-PALSAR data, (d) time-series surface deformation using ALOS-PALSAR data.

occurred. Despite this lack of volcanic activity, Augustine Volcano can be regarded as an area of surface displacement; thus, its volcanic activity should be monitored continuously.

4.3. Veniaminof, Shishaldin and Makushin Volcanoes

Veniaminof Volcano showed weak volcanic activity (Volcanic Explosivity Index [VEI] score of 1) from 2006 to 2008. Time series analysis of the Veniaminof volcanic area revealed slight displacement of the entire volcanic island, of within 0.1 cm. It is not clear whether the displacement was caused by volcanic activity (Figs. 4a and b).

Figure 4c shows the location of Shishaldin Volcano, and Figure 4d is the time-series of surface displacement based on various observation points. Shishaldin Volcano features small and frequent eruptions rather than large eruptions; this pattern was seen during the study period. The deformation occurring between 2009 and 2010 was determined to have been caused by activities such as small-scale volcanic earthquakes.

Makushin last erupted in 2001 and shows surface deformation irrespective of volcanic eruption although there is a pattern of subsidence (Figs. 4e and f).

4.4. Okmok Volcano

Figure 5a shows the location of Okmok Volcano, Figure 5b is the time-series of surface displacement based on various observation points, Figure 5c is the differential interference map generated using ALOS-PALSAR images, and Figure 5d is the time-series of deformation. Okmok Volcano has shown continuous surface displacement since the eruption in 2008. In addition, surface displacement due to volcanic activity is apparent in craters. Subsidence can be seen on the west side of the volcano, while surface elevation is seen to the east. The time-series analysis in Figure 5d shows that subsidence occurred after the 2008 eruption (VEI score of 4).

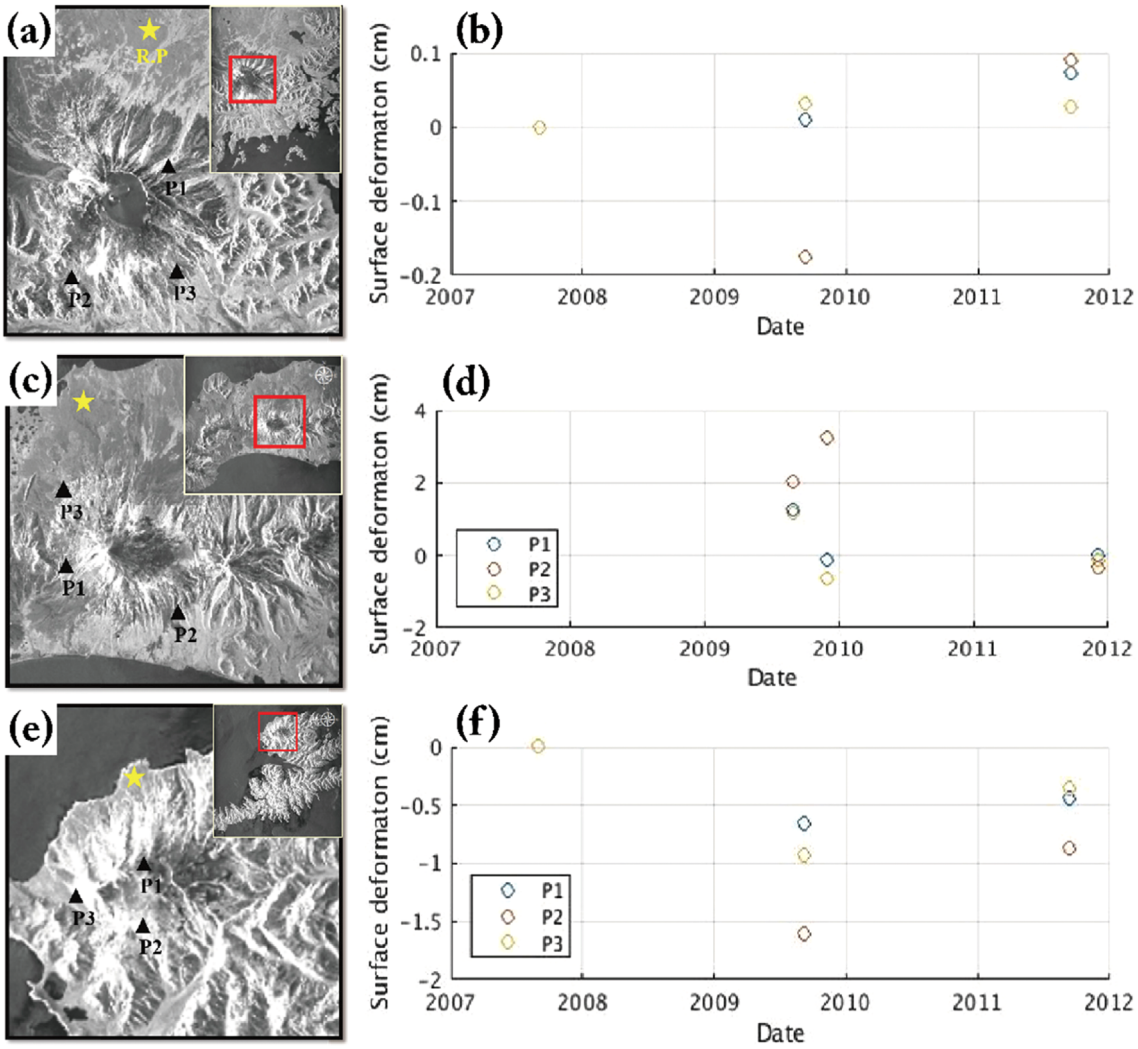

Fig. 4. Results for different volcano types; (a) location of Veniaminof Volcano using SAR data, (b) surface deformation at the observation point for Veniaminof, (c) location of Shishaldin Volcano using SAR data, (d) surface deformation at the observation point for Shishaldin, (e) location of Makushin Volcano using SAR data, (f) surface deformation at the observation point for Makushin.

4.5. Cleveland, Korovin and Kanaga Volcanoes

Figure 6a shows the location of Cleveland Volcano and Figure 6b is the time-series of surface displacement based on various observation point. Cleveland Volcano experienced small-scale eruptions from 2006 to 2012. Time-series analysis based on ALOS images revealed subsidence. Thus, surface displacement can be determined to have occurred due to volcanic eruption.

Figure 6c shows the location of Korovin Volcano and Figure 6d shows the time-series of surface displacement based on various observation points. Korovin Volcano shows subsidence regardless of the lack of any volcanic activity since the 2006 eruption (VEI score of 1).

Kanaga experienced no eruptions between 2006 and 2010. Continuous displacement is difficult to discern; however, displacement can be seen in one location, although it is not certain that this was caused by volcanic activity (Figs. 6e and f).

4.6. Seguam Volcano

Seguam (Fig. 7a) was the most active of the study volcanoes around 1993, with surface displacements observed between 1992 and 2010 on ERS images. The volcanic peaks are located on the east and west sides of the volcano. Subsidence can be observed on the west side, with the surface rising in the east. Seguam last erupted in 1993, from its western crater. Ground subsidence occurred due to compaction after the eruption. The surface elevation is assumed to be due to volcanic activity. Surface displacement is clearly visible in the area around Seguam Volcano, even without any recent eruptions (Fig. 7b).

The purpose of this study was to analyze the correlation between surface displacements of volcanoes in Alaska (Fig. 8a), calculated

https://doi.org/10.1007/s12303-018-0050-z

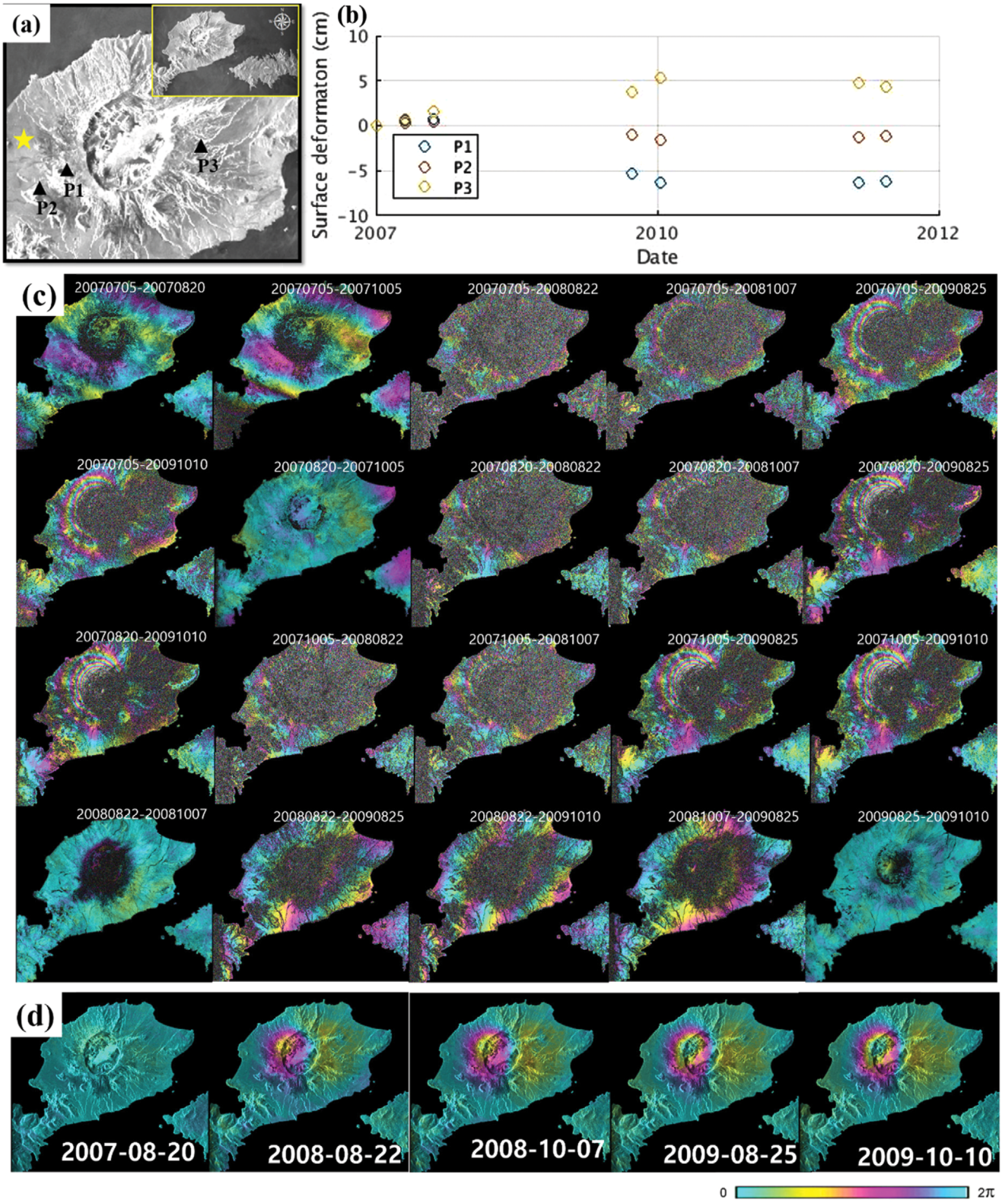

Fig. 5. Results for Okmok Volcano; (a) location of Okmok Vlcano using SAR data, (b) surface deformation at the observation point, (c) differential interference map using ALOS-PALSAR data, (d) time-series surface deformation using ALOS-PALSAR data.

by time-series analysis, and patterns of eruption based on radar satellite images. Time-series displacements of currently active volcanoes were seen on the satellite images (Fig. 8b).

The sensitivity value, i.e., the probability that a volcanic eruption

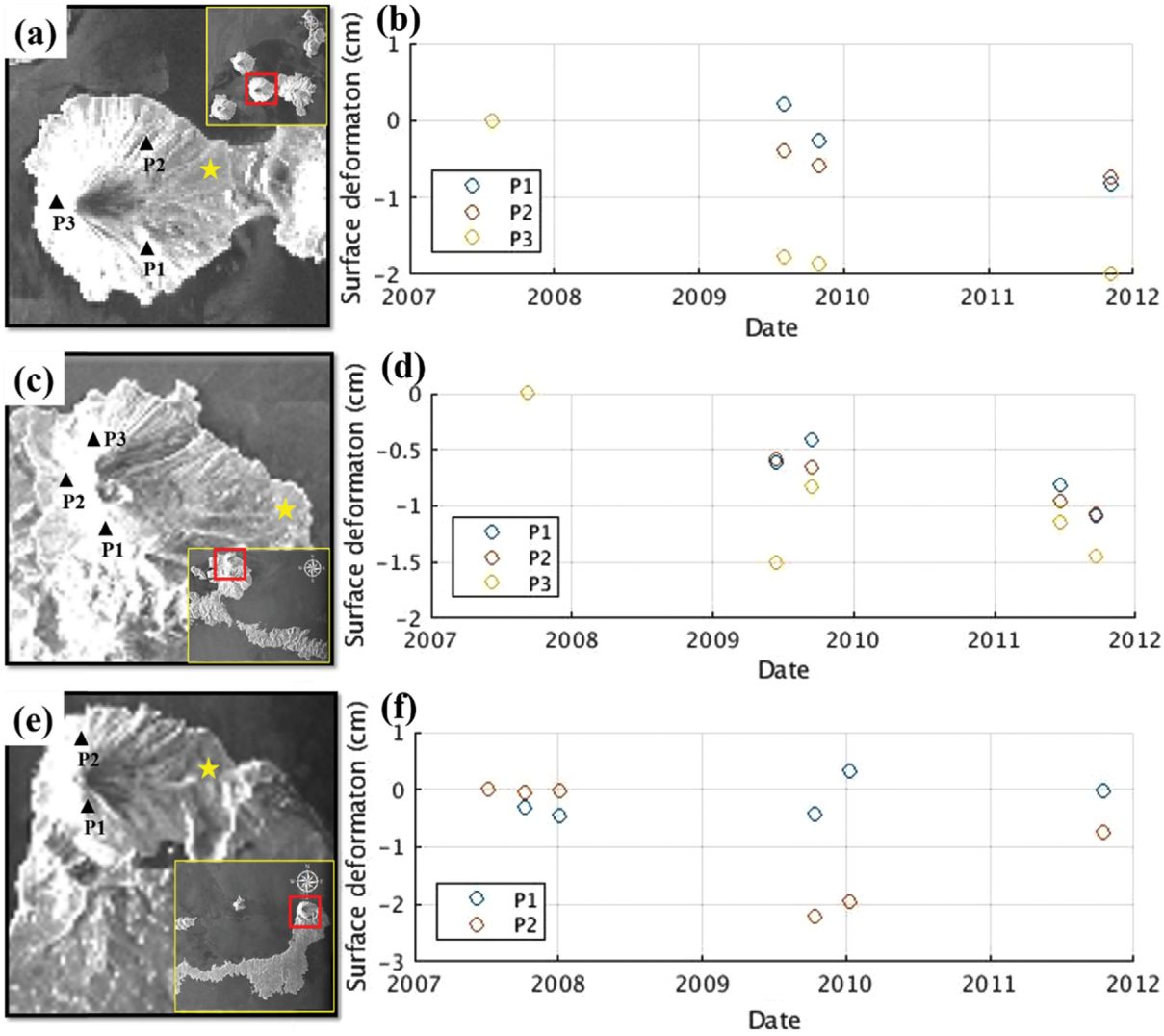

Fig. 6. Results for different volcanoes; (a) location of Cleveland Volcano using SAR data, (b) surface deformation at the observation point for Cleveland, (c) location of Korovin Volcano using SAR data, (d) surface deformation at the observation point for Korovin, (e) location of Kanaga Volcano using SAR data, (f) surface deformation at the observation point for Kanaga.

will be accompanied by displacement, was 1 based on the results of this study, meaning that there is always displacement when a volcano erupts. Specificity had a value of 0.25, while the overall PPV and NPV were 0.67 and 1, respectively. These results show that differentiation can occur without surface displacement.

5. CONCLUSION

In this study, recent volcanic activity in Alaska, one of the most active volcanic regions in the world, was analyzed using radar satellite images. The volcanic eruption histories of 10 recently active volcanoes in Alaska were studied. During periods of general volcanic activity, surface displacements were observed and correlated with those seen during actual eruptions. ERS-1/2 (1993–2001) and ALOS PALSAR (2007–2011) image data were collected to observe surface displacements at the study sites. Time-series analysis was performed for each volcano by applying an SBAS algorithm tailored to that site and based on the collected images. SBAS requires pairs of images that are not highly spatially correlated. However, few such image pairs were available from ERS-1/2 and ALOS data, rendering it difficult to observe continuous displacement using the SBAS technique. However, the images obtained were sufficient for observing spatial displacements and calculating time-series thereof. In this study, we applied the positive and negative predictive values method to time-series analyses and volcanic history data based on radar satellite images. An overall sensitivity value of 1 and an NPV of 1, were obtained, indicating that in no case does surface displacement fail to occur while a volcano is active. The calculated specificity and PPV values were 0.25 and 0.67, respectively, showing that

https://doi.org/10.1007/s12303-018-0050-z

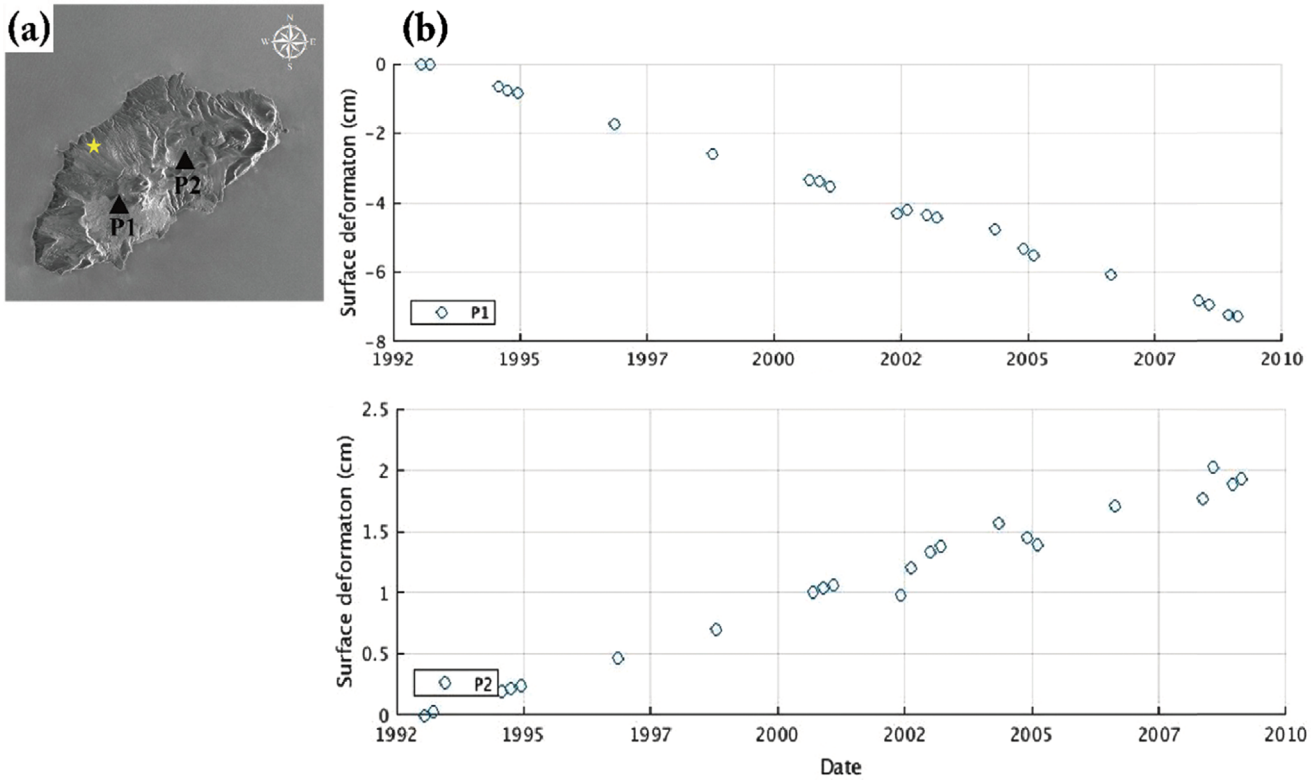

Fig. 7. (a) Results for Seguam Volcano; time-series surface deformation using ERS-1/2 data, (b) surface deformation at the observation points P1 and P2.

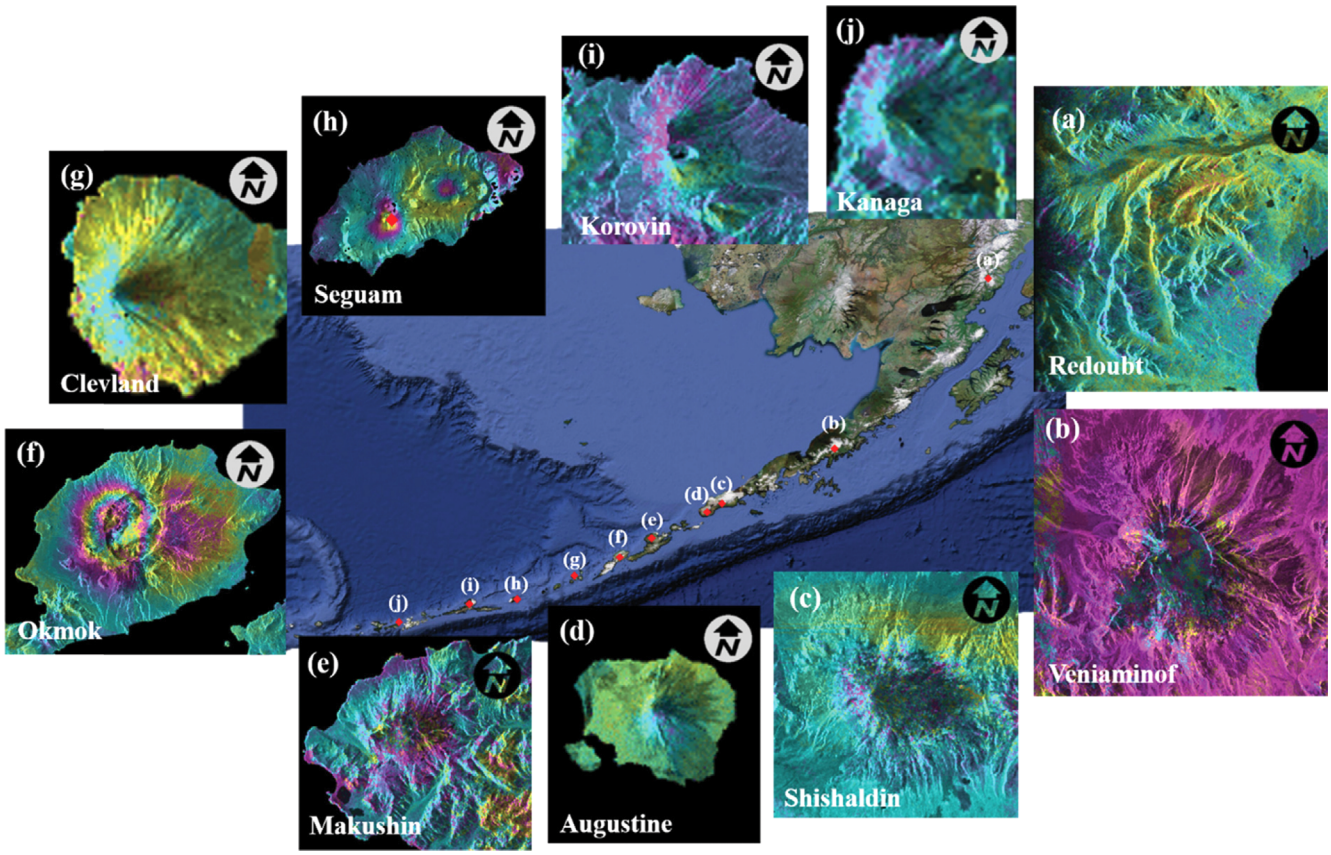

Fig. 8. Average time-series deformation values at each volcano; (a) Redoubt, (b) Veniaminof, (c) Shishaldin, (d) Augustine, (e) Makushin, (f) Okmok, (g) Cleveland, (h) Seguam, (i) Korovin, and (j) Kanaga.

surface displacement can occur without distinctive activity. The correlation between patterns of volcanic eruption and surface displacement could be further elucidated through analysis of other factors that are influenced by volcanic activity, to build upon the results of this study.

ACKNOWLEDGMENTS

This research was supported by National Research Foundation of Korea (NRF) grants funded by the Korean government (MSIP) (Nos. 2017R1A2B4003258 and 2015M1A3A3A02013416).

REFERENCES

Begét, J.E. and Kowalik, 2006, Confirmation and calibration of computer modeling of tsunamis produced by Augustine Volcano, Alaska. Science of Tsunami Hazards, 24, 257–266

Berardino, P., Fornaro, G., Lanari, R., and Sansosti, E., 2002, A new algorithm for surface deformation monitoring based on small baseline differential interferograms. IEEE Transactions on Geoscience and Remote Sensing, 40, 2375–2383.

Biggs, J., Ebmeier, S.K., Aspinall, W.P., Lu, Z., Pritchard, M.E., Sparks, R.S.J., and Mather, T.A., 2014, Global link between deformation and volcanic eruption quantified by satellite imagery. Nature Communications, 5, 3471. https://doi.org/10.1038/ncomms4471

Cho, M., Zhang, L., and Lee, C.W., 2013, Monitoring of volcanic activity of Augustine Volcano, Alaska using TCPInSAR and SBAS time-series techniques for measuring surface deformation. Korean Journal of Remote Sensing, 29, 21–34. (in Korean with English abstract)

De Angelis, S., Fee, D., Haney, M., and Schneider, D., Detecting hidden volcanic explosions from Mt. Cleveland Volcano, Alaska with infrasound and ground-couples airwaves. Geophysical Research Letters, 39, L21312. https://doi.org/10.1029/2012GL053635

Dixon, J.P. and Power, J.A., 2009, The January 2006 volcanic-tectonic earthquake swarm at Mount Martin, Alaska. In: Haeussler, P.J. and Galloway, J.P. (eds.), Studies by the U.S. Geological Survey in Alaska, 2007. U.S. Geological Survey Professional Paper, 1760-D, 17 p.

Ferretti, A., Prati, C., and Rocca, F., 2000, Nonlinear subsidence rate estimation using permanent scatterers in differential SAR interferometry. IEEE Transactions on Geoscience and Remote Sensing, 38, 2202–2212.

Ferretti, A., Prati, C., and Rocca, F., 2001, Permanent Scatterers in SAR Interferometry. IEEE Transactions on Geoscience and Remote Sensing, 39, 8–20.

Guffanti, M.C. and Miller, T.P., 2013, A volcanic activity alert-level system for aviation –review of its development and application in Alaska. Natural Hazards, 69, 1519–1533.

Hong, S.H., Wdowinski, S., Kim, S.W., and Won, J.S., 2010, Multi-temporal monitoring of wetland water levels in the Florida everglades using interferometric synthetic aperture radar (InSAR). Remote Sensing of Environment, 114, 2436–2447.

Jung, H.C., Kim, S.W., Jung, H.S., Min, H.D., and Won, J.S., 2007, Satellite observation of coal mining subsidence by persistent scatterer analysis. Engineering Geology, 92, 1–13.

Jung, H.S., Lee, C.W., Park, J.W., Kim, K.D., and Won, J.S., 2008, Improvement of small baseline subset (SBAS) algorithm for measuring time-series surface deformations from differential SAR interferograms. Korean Journal of Remote Sensing, 24, 165–177. (in Korean with English abstract)

Kienle, J. and Shaw, G.E. 1979, Plume dynamics, thermal energy and long-distance transport of vulcanian eruption clouds from Augustine Volcano, Alaska. Journal of Volcanology and Geothermal Research, 6, 139–164.

Kim, S.W., 2010, A comparison of InSAR techniques for deformation monitoring using multitemporal SAR. Korean Journal of Remote Sensing, 26, 143–151. (in Korean with English abstract)

Kim, S.W. and Cho, M., 2011, Persistent scatterer selection and network analysis for X-band PSInSAR. Korean Journal of Remote Sensing, 27, 521–534. (in Korean with English abstract)

Kim, S.W., 2012, Development of unwrapped InSAR phase to height conversion algorithm. Korean Journal of Remote Sensing, 28, 227–235. (in Korean with English abstract)

Lange, K. and Brunner, E., 2013, Analysis of predictive values based on individual risk factors in multi-modality trials. Diagnostics, 3, 109–209.

Lee, C.W., Lu, Z., Jung, H.S., Won, J.S., and Dzurisin, D., 2010, Surface deformation of Augustine Volcano (Alaska), 1992–2005, from multiple-interferogram processing using a refined SBAS InSAR approach. In: Power, J.A. and Coombs, M.L. (eds.), The 2006 Eruption of Augustine Volcano, Alaska. USGS Professional Paper, 1769. https://doi.org/ 10.3133/pp176918

Lee, C.W., Lu, Z., and Jung, H.S., 2012, Simulation of time-series surface deformation to validate a multi-interferogram InSAR processing technique. International Journal of Remote Sensing, 33, 7075–7087.

Lee, C.W., Lu, Z., and Kim, J.W., 2017, Monitoring Mount Sinabung in Indonesia using multi-temporal InSAR. Korean Journal of Remote Sensing, 33, 37–46. (in Korean with English abstract)

Lu, Z., Masterlark, T., and Dzurisin, D., 2005, Interferometric synthetic aperture radar study of Okmok Volcano, Alaska, 1992–2003: Magma supply dynamics and post-emplacement lava flow deformation. Journal of Geophysical Research, 110, B02403. https://doi.org/10.1029/2004JB003148

Lu, Z., Wicks, C., Dzurisin, D., and Power, J., 2005a, InSAR studies of Alaskan volcanoes, Korean Journal of Remote Sensing, 21, 59–72.

Miller T.P., McGimsey R.G., Richter D.H., Riehle, J.R., Nye, C.J., Yount, M.E., and Julie A.D., 1998, Catalog of the historically active volcanoes of Alaska. U.S. Geological Survey Open-File Report 98–582, 85 p.

McGimsey, R.G., Neal, C.A., and Girina, O., 2003, 1998 volcanic activity in Alaska and Kamchatka; summary of events and responses of the Alaskan Volcano Observatory. U.S. Geological Survey Open-File Report 2003–423, 35 p.

McGimsey, R., Neal, C., Dixon, J., Ushakov, S., and Rybin, A., 2007, 2005 volcanic activity in Alaska, Kamchatka, and the Kurile Islands: summary of events and responses of the Alaskan Volcano

Observatory. U.S. Geological Survey Scientific Investigations Report 2007–5269, 94 p.

Neal, C.A., McGimsey, R.G., Dixon, J.P., Cameron, C.E., Nuzhaev, A.A., and Chibisova, M., 2011, 2008 volcanic activity in Alaska, Kamchatka, and the Kurile Islands: summary of events and responses of the Alaskan Volcano Observatory. U.S. Geological Survey Scientific Investigations Report 2010–5243, 94 p.

Parikh, R., Mathai, A., Parikh, S., Sekhar, G.C., and Thomas, R., 2008, Understanding and using sensitivity, specificity and predictive values. Journal of Ophthalmology, 56, 45–50.

Waythomas, C.F. and Waitt, R.B., 1998, Preliminary volcano-hazard assessment for Augustine Volcano, Alaska. U.S. Geological Survey Open-File Report 98–106, 39 p.

Waitt, R.B. and Begét, J.E., 2009, Volcanic processes and geology of Augustine Volcano, Alaska, U.S. Geological Survey Professional Paper 1762, 78 p.

Yang C.S., Zhang, Q., Zhao, C.Y., Wang, Q.L., and Ji, L.Y., 2014, Monitoring land subsidence and fault deformation using the small baseline subset InSAR technique: a case study in the Datong Basin, China. Journal of Geodynamics, 75, 34–40.